MECHANISM AND COUNTERMEASURES OF WAVE OVERTOPPING FOR LONG-PERIOD SWELL IN COMPLEX BATHYMETRY

Hiroaki Kashima[1] and Katsuya Hirayama[1]

Recently, coastal disasters due to long-period swells induced by heavy storms and catastrophic typhoons have increased at Japanese coasts and harbors. Long-period swells are more susceptible to the bottom bathymetry of the offshore deep water region and their wave heights locally increase due to the concentration of wave energy caused by the complex bottom bathymetry in the relatively shallow water region. In addition, the wave overtopping rate may increase due to the long waves in front of the seawall induced by the long-period swells. However, the spatial relationship between wave characteristics and wave overtopping discharges in the complex bathymetry are not well known owing to a lack of detailed measurements. In this study, model experiments were conducted by using a large basin to investigate the spatial characteristics of wave transformation and wave overtopping focusing on the heavy wave overtopping damages caused by the arrivals of long-period swells at the Shimoniikawa Coast in 2008. Effective countermeasures against wave overtopping are also discussed based on their characteristics.

Keywords: long-period swell; long wave; wave overtopping; seawall; jetty; submerged breakwater

INTRODUCTION

Many Japanese harbors directly face the Pacific Ocean and the Japan Sea where both high wind waves and swells often occur due to heavy storms. Although breakwaters and seawalls have been designed to protect against these severe waves, coastal disasters due to long-period swells induced by heavy storms and catastrophic typhoons have increased at Japanese coasts and harbors recently. For example, the collapses of seawalls and inundation behind the defending reclaimed area in Kuji Harbor were caused by heavy wave overtopping due to 14.5 s swells in 2006 (Hirayama et al., 2008). The seawall along the Shonan Coast in the Odawara region facing the Pacific Ocean was damaged by 14.2 s swells in 2007. Moreover, severe damage to property and inhabitants in the Ashizaki district of Nyuzen town on the Shimoniikawa Coast was caused by long-period swells with high wave heights in 2008 (Kawasaki et al., 2008). Thus, it is necessary to take countermeasures urgently to reduce the severe damage caused by long-period swells.

Fortunately, long-period swells have been observed at several wave observation stations along the Japanese coastline (Kashima et al. 2009). These long-period swells have narrower-band spectra than those of wind waves, and wave groupings with high waves can appear in the time series of their wave profiles. They steepen due to wave shoaling and refraction under the effects of bottom bathymetry in the deep water region because their relative water depth is shallower than that of wind waves. Moreover, long-period swells with wave groupings have effects on wave overtopping discharges on a seawall. Kashima and Hirayama (2010) have suggested that the long waves associated with the development of wave groupings are generated by second nonlinear interactions between their component waves. Furthermore, wave overtopping discharges on a seawall increase due to the effect of instantaneous water surface elevation as a result of the specific long waves in front of the seawall for unidirectional long-period swells. Therefore, it is important to consider not only the characteristics of long-period swells with wave groupings but also long waves when discussing wave overtopping discharges for long-period swells.

There have been several studies on the characteristics of long-period swells. Kashima and Hirayama (2009) discussed the difference between the transformation of long-period swells and wind waves on the complex bathymetry including the deep water region. Long-period swells are more susceptible to the bottom bathymetry of the deep water region than wind waves and their wave heights locally increase due to the concentration of wave energy in relatively shallow water. Tajima et al. (2009) and Fukase et al. (2010), analyzing observed data and focusing on the damage features, stated that the concentration of wave energy on the damaged area is caused by the interactions among waves, bathymetry and near shore currents. In particular, the slowly varying wave-induced nearshore currents have a significant impact on the local concentration of waves around sharply-changing coastal bathymetries. On the other hand, Fukase et al. (2009) investigated the generation of long waves induced by nonlinear interactions between the component waves of long-period swells at the Shimoniikawa

[1] Coastal and Ocean Engineering Field, Port and Airport Research Institute, 3-1-1 Nagase, Yokosuka, Kanagawa, 239-0826, Japan

Coast. However, these discussions mainly focused on the wave energy concentration due to bottom bathymetry. The spatial relationship between wave characteristics and wave overtopping discharges in complex bathymetry such as the Shimoniikawa Coast is not well known owing to a lack of detailed measurements.

The purpose of this study is to investigate the mechanism and countermeasures of wave overtopping for long-period swells at the Shimoniikawa Coast, experimentally. First, spatial measurements of wave characteristics and wave overtopping discharges are carried out by using a wave basin installed with a complex bottom bathymetry model focused on the Shimoniikawa Coast. Second, effective countermeasures for wave overtopping discharges are discussed based on the spatial characteristics of waves around the damaged area.

WAVE OVERTOPPING EXPERIMENTS

Experimental Setup

The model experiments were conducted in a large basin that is 48.0m times 25.0m long and 1.5m deep located at the Port and Airport Research Institute in Japan. This basin has 100 wave paddles with active wave absorbers in an L-shape layout (Fig. 1(a)). A complex bathymetry model of the Shimoniikawa Coast including submerged and detached breakwaters located in front of a seawall was installed (see Fig. 1(b)). The experimental scale was 1/100 by Froude's similarity rule. Details of the experimental setup are shown in Fig. 2. The horizontal (x) and vertical (y) axes are the distance from the ridge line (y = 0.0 km) and the wave generator which is positioned corresponding to offshore (x = 0.0 km), respectively. The contour lines indicate water depth at intervals of 2.5 m. The circles and crosses indicate capacitance-type wave gauges and electromagnetic velocity meters, respectively. Numbers in parentheses indicate the water catchment tank number. The horizontal dotted lines indicate measurement lines used in the following discussion.

Forty nine capacitance-type wave gauges were installed in the range from offshore to onshore to measure the spatial distribution of wave statistics and twelve electromagnetic velocity meters were installed in the relatively shallower water region to examine the wave characteristics near the seawall. Moreover, seven water catchment tanks were installed behind the seawall to measure the spatial distribution of wave overtopping discharges.

Experimental Conditions

The model experiments were performed with the estimated waves from observed data. The wave data was observed at the Tanaka wave observation station near the damaged area. The significant wave height $H_{1/3}$ and wave period $T_{1/3}$ were estimated to be 5.97 m and 13.9 s offshore. The frequency spectral shape was chosen as the JONSWAP-type spectrum with γ = 4.0 based on the work of Hirayama et al. (2009). The offshore water depth h was set at 90.2 m in consideration of the tidal level when severe damage occurred. The principal wave direction θ_p and the spreading parameter S_{max} were set at an angle rotated 15 degrees clockwise to the positive direction of x (θ_p = N18.5E) and S_{max} = 999 as a swell condition.

The data of the water surface elevation and the fluid velocity were recorded at 25 Hz for up to

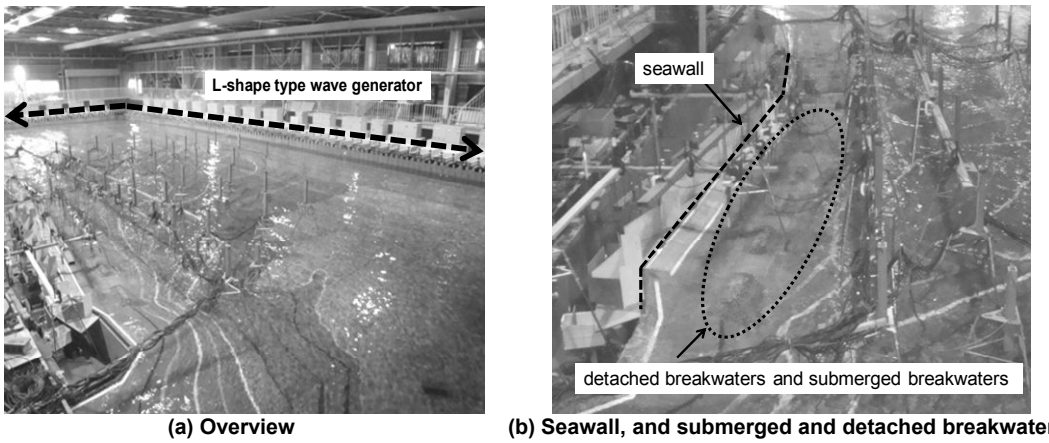

(a) Overview (b) Seawall, and submerged and detached breakwaters

Figure 1. Experimental wave basin

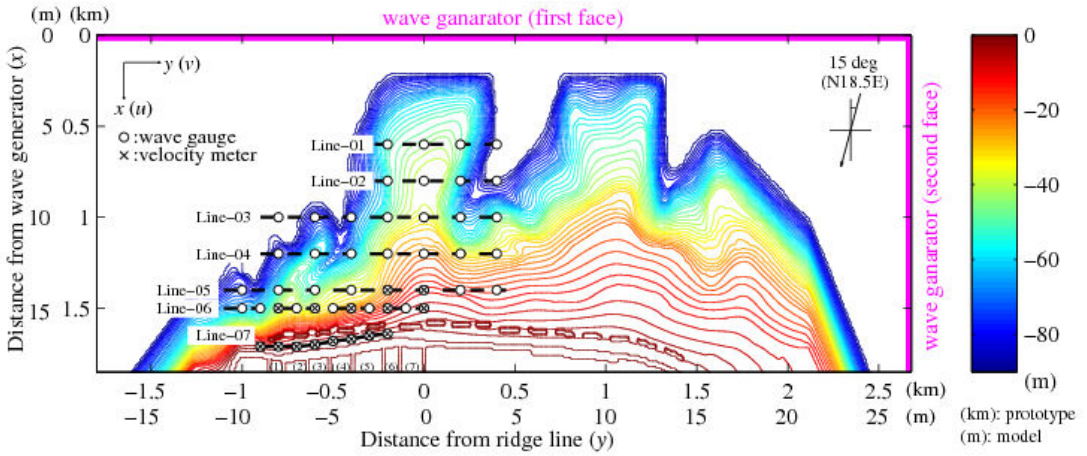

Figure 2. Illustration of experimental setup (contour lines: water depth, circles: capacitive wave gauges, crosses: electromagnetic velocity meters, numbers in parentheses: water catchment tank, dashed lines: measurement lines)

1000 individual waves by using the capacitance-type wave gauges and the electromagnetic velocity meters. In our analysis, first, short waves of less than 30 s and long waves of 30-300 s were estimated from the measured wave profiles by applying the Fast Fourier Transformation method and band-pass filtering. Second, each significant wave height was calculated by zero-up crossing for the wave profiles of the short and long waves extracted by the inverse Fast Fourier Transformation method, respectively. The variations of wave set-up and wave overtopping rate on the seawall were calculated as time-averaged values of water surface elevation and wave overtopping discharge in the water catchment tank, respectively.

RESULTS AND DISCUSSION

Wave Characteristics and Wave Overtopping

First, the wave characteristics in the event of severe disasters caused by the arrival of long-period swells were investigated in order to comprehend the spatial distributions of the wave overtopping at the Shimoniikawa Coast. Fig. 3 shows the spatial distributions of the short and long wave height and the wave set-up made by spline interpolation of wave statistics at each measurement point. The color contours indicate the statistics of each wave and the lines are bathymetric lines at intervals of 2.5 m. The short waves propagating from offshore concentrate on the ridge (y = −0.3 to 0.0 km) due to the effects of refraction and wave shoaling, and their heights become larger than 7.0 m. Moreover, the short wave height on the small ridge (y = −0.7 km and x = 1.4 km) increases locally. However, the short wave height behind the submerged and detached breakwaters on the steep slope side (y = −0.8 to −0.4 km) decreases due to the wave breaking. On the other hand, as the water depth becomes shallower, the long wave height increases and reaches 2.0 m behind the submerged and detached breakwaters. Moreover, the wave set-up also increases with a similar tendency to the long wave height. Therefore, it is considered that the waves with high wave height become more than 7.0 m on the ridge, and remarkable long waves and wave set-up are generated in front of the seawall including the damaged seawall near y = −0.8 km when severe disasters were caused by the arrival of long-period swells.

Second, to discuss the wave overtopping characteristics, Fig. 4 shows the relationship between the wave statistics in front of the seawall and the wave overtopping rate on the seawall. Each figure shows the short wave height (H_S), long wave height (H_L), variation of wave set-up (η_{bar}) and wave overtopping rate (q) from the top. The circles and crosses indicate the data in front of the submerged and detached breakwaters (Line-06) and the seawall (Line-07), respectively and the squares indicate the wave overtopping rate. As already shown in Fig. 3, in front of the submerged and detached breakwaters (Line-06), the short wave height becomes larger on the mild slope side due to the effects of refraction and wave shoaling, and the long wave height becomes larger in the shallow water region. On the other hand, in front of the seawall (Line-07), the short wave height becomes smaller due to waves breaking, and both long wave height and the variation of wave set-up increase rapidly in front of the seawall. Moreover, the wave set-up increases in the surf zone on the mild slope side and behind the submerged

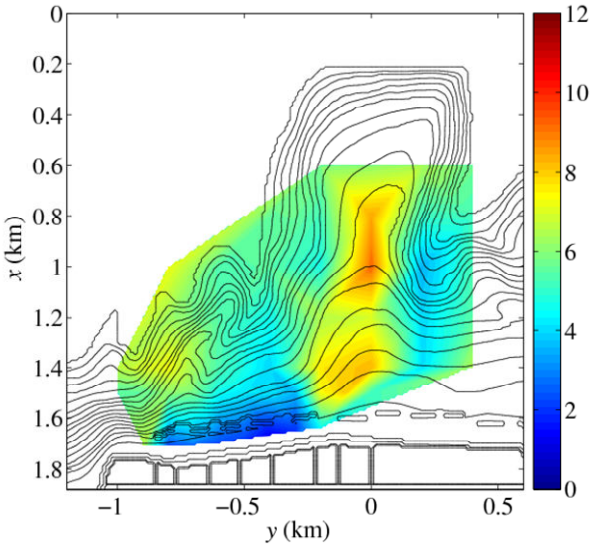

(a) Short wave height

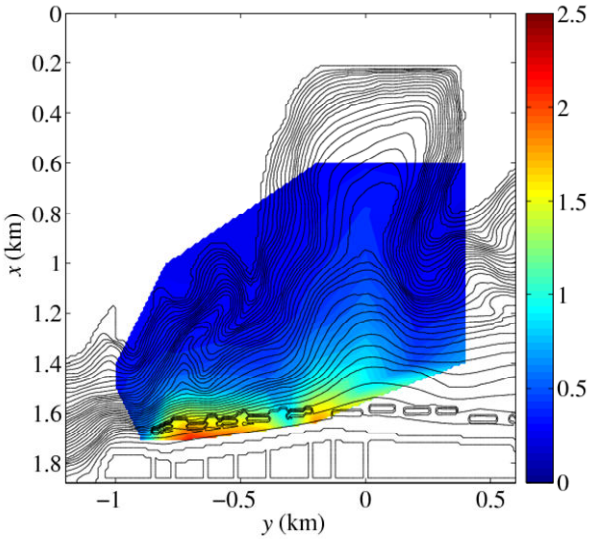

(b) Long wave height

(c) Variation of wave set-up

Figure 3. Spatial distributions of wave statistics in the event of severe disaster caused by the arrival of long-period swells (color contour: each wave statistics, line: bathymetric line at intervals of 2.5 m)

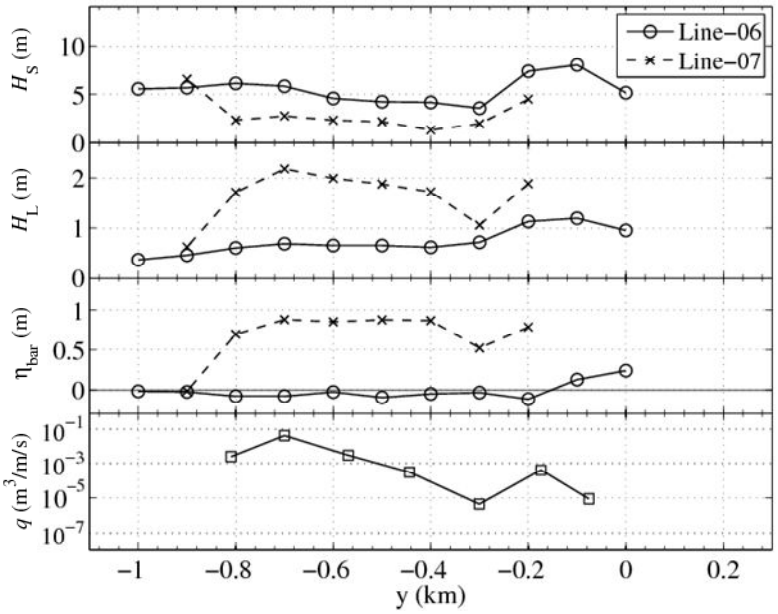

Figure 4. Relationship between wave statistics in front of the seawall and wave overtopping rate on the seawall (circles: data in front of the submerged and detached breakwaters, crosses: data in front of the seawall, squares: wave overtopping rate on the seawall)

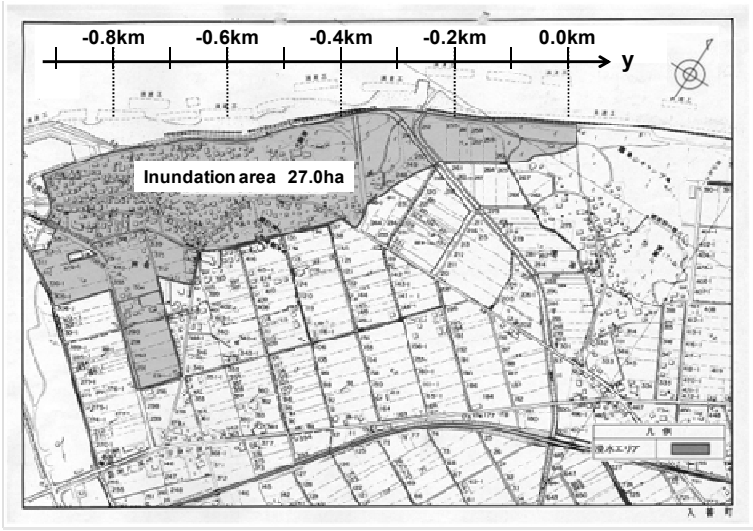

Figure 5. Inundation area by field survey of damages (gray area: inundation area)

and detached breakwaters on the steep slope side, and decreases at the border between the two slopes (y = −0.3 km).

The wave overtopping rate on the seawall at y = −0.8 to −0.7 km, which is the most severely damaged area, is the largest among the measurement points for wave overtopping discharge and generally becomes smaller toward the northwest (in a positive direction on the y-axis). Moreover, the distribution of wave overtopping rate is similar to that of the long wave height and is in good agreement with the inundation area obtained by the field survey of damages as shown in Fig. 5. According to the results of Kashima and Hirayama (2010), the wave overtopping rate becomes larger due to the effects of the long waves induced by wave grouping of short waves in front of the seawall for unidirectional long-period swells. Therefore, these experimental results imply that the long waves in front of the seawall have an important effect on the increase of wave overtopping rate on the seawall. Details of the long wave characteristics in front of the seawall are discussed in the next section.

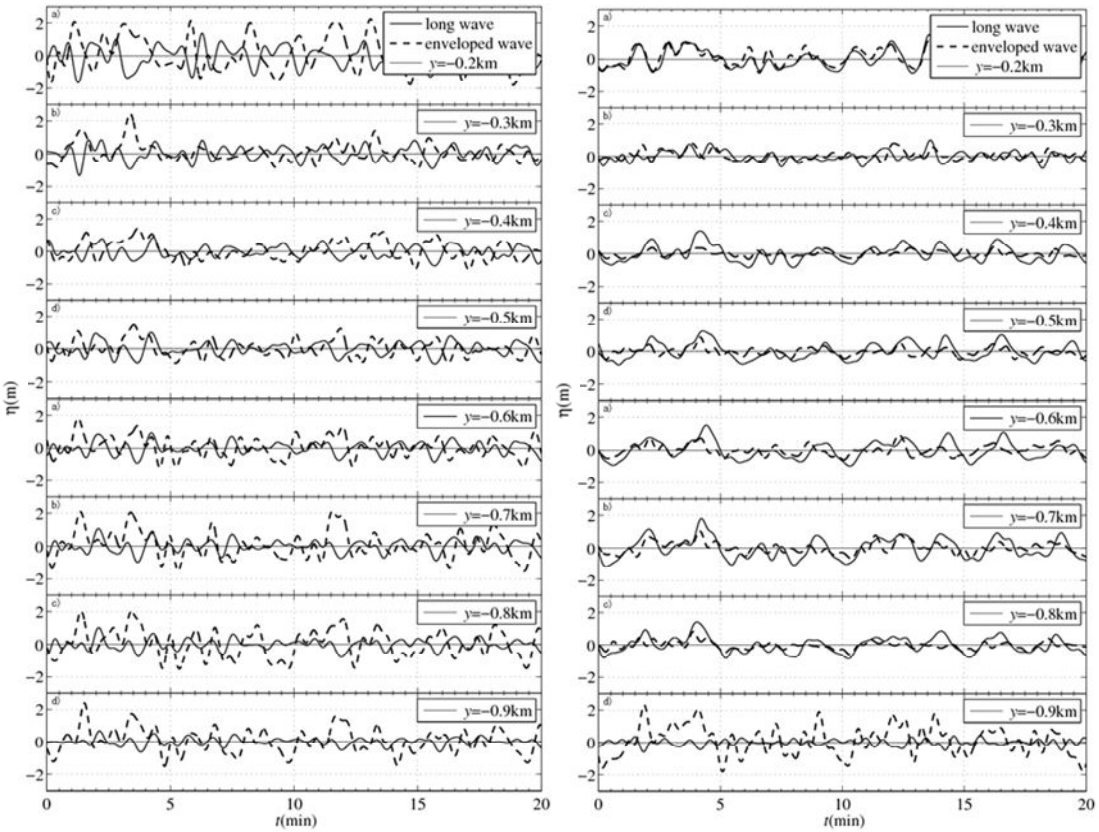

(a) In front of the submerged and detached breakwaters **(b) In front of the seawall**

Figure 6. Time series variation of long waves and the enveloped waves for short waves (solid line: long waves, dashed line: enveloped waves)

Behavior of Long Waves in Front of Seawall

In the previous section, we found that not only the short waves from offshore but also the long waves in front of the seawall are very important factors for the increase of wave overtopping rate on the seawall. In this section, the behavior of the long waves in front of the seawall is investigated based on the time series variation and spectral distributions of water surface elevation and fluid velocity.

Fig. 6 shows the time series variation of water surface elevation of the long waves and the enveloped waves for the short waves in front of the submerged and detached breakwaters and the seawall, respectively. The enveloped waves for the short waves were defined by List (1992). The solid and dashed lines indicate the long waves and the enveloped waves for the short waves, respectively. The horizontal axis is time (t) and the vertical axis is the water surface elevation of two waves (η). The amplitude of the long waves in front of the submerged and detached breakwaters is expanded by twice for convenience of explanation because it is extremely small in Fig. 6(a). These figures show that the profile of the long waves is not similar to that of the enveloped waves for the short waves in front of the submerged and detached breakwaters from $y = -0.9$ to -0.2 km (Fig. 6(a)). On the other hand, in front of the seawall, the amplitude and phase of the long waves almost match those of the enveloped waves for the short waves from $y = -0.3$ to -0.2 km (Fig. 6(b)). However, there is a small difference between the appearance time of the crest amplitudes of the two waves from $y = -0.8$ to -0.4 km. Moreover, the phase of the enveloped waves for the short waves from $y = -0.8$ to -0.4 km in front of both the submerged and detached breakwaters and the seawall mutually correspond among the measurement points.

Fig. 7 shows the spatial variations of the cross-correlation coefficient between the long waves and the enveloped waves for the short waves from offshore to onshore. The horizontal axis is time lag (τ) and the color contours indicate the cross-correlation coefficient between two waves (R). The vertical dashed line corresponds to $\tau = 0.0$ s and the horizontal dotted line from $y = -0.8$ to -0.2 km in each figure indicates the location of the submerged and detached breakwaters. The cross-correlation

coefficient between two waves is given by:

$$R(\tau) = \frac{< A(t)^2 \eta_L(t+\tau) >}{\sigma_{A^2} \sigma_{\eta_L}} \quad (1)$$

where $A(t)$ and $\eta_L(t)$ are the wave profiles of the enveloped waves for the short waves and the long waves, respectively. The brackets <> indicate the ensemble-averaged value for time (t). σ_{A2} and $\sigma_{\eta L}$ are the standard deviations for the enveloped waves for the short waves and the long waves, respectively. A negative correlation can be observed from x = 0.6 km up to x = 1.4 km at τ = 0.0 s on the ridge (y = 0.2 to 0.4 km). On the other hand, the cross-correlation coefficient along τ = 0.0 s is essentially inverted close to the shoreline in comparison to the offshore situation from y = −0.8 to −0.2 km. Offshore, the long waves are negatively correlated with the enveloped waves for the short waves at τ = 0.0 s, while the cross-correlation coefficient at near-zero time lags is dominantly positive in the near shore region.

Kashima and Hirayama (2010), List (1992) and Janssen and Battjes (2003) reported in unidirectional irregular wave experiments that the long waves are negatively correlated with the enveloped waves for the short waves and that long waves bound in wave grouping including the short waves are generated offshore, but the cross-correlation coefficient between two waves is dominantly positive in the surf zone and near shore region. This means that the long waves bound in wave grouping are released in the wave breaking process and the free long waves propagate in the surf zone. Thus the behavior of the long waves in this experiment can be summarized as follows. First, on the mild slope side (y = −0.3 to −0.2 km), the long waves are negatively correlated with the enveloped waves for the short waves and the long waves bound in wave grouping are remarkably generated in front of the submerged and detached breakwaters. Thus, it is supposed that long waves bound in wave grouping are released due to the wave breaking behind the submerged and detached breakwaters because the profile of the long waves almost matched that of the enveloped waves for the short waves. These results closely correspond to the results of unidirectional irregular wave experiments by List (1992) and Kashima and Hirayama (2010), and imply that unidirectional long waves are generated in front of the seawall. Second, on the steep slope side (y = −0.8 to −0.4 km), the behavior of the long waves is similar to that on the mild slope side (y = −0.3 to −0.2 km) in front of the submerged and detached breakwaters. It is also expected that the long waves bound in wave grouping are released due to the wave breaking behind the submerged and detached breakwaters, the same as the results on the mild slope side, but there are significant differences between the two waves in terms of their amplitudes and phases. Therefore, there is a clear difference between the behavior of the long waves on the mild slope side and on the steep slope side.

In order to check the behavior of the long waves in front of the seawall in detail, Fig. 8 shows the spectra of the water surface elevation and two-directional fluid velocities. The horizontal axis is the frequency (f) and the vertical axis is the energy density of water surface elevation and two-directional fluid velocities (S_η, S_u and S_v), respectively. The vertical dashed line indicates the boundary frequency (1/30 Hz) between the short and long waves. First, the energy density of the long waves is smaller (i.e., $S_\eta = O(10^1)$) and the energy density of the fluid velocity along the shore for the long waves is larger

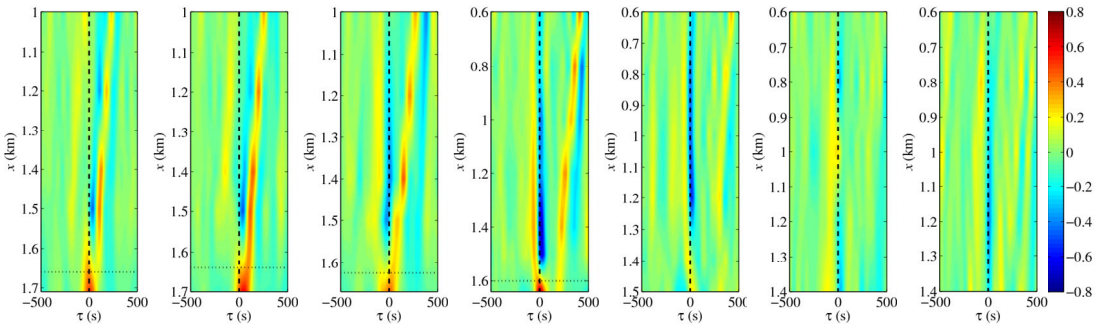

Figure 7. Spatial variations of the cross-correlation coefficient between the long waves and the enveloped waves (color contour: cross-correlation coefficient, vertical dashed line: τ = 0 s, horizontal dotted line from y = −0.8 to −0.2 km: location of the submerged and detached breakwaters)

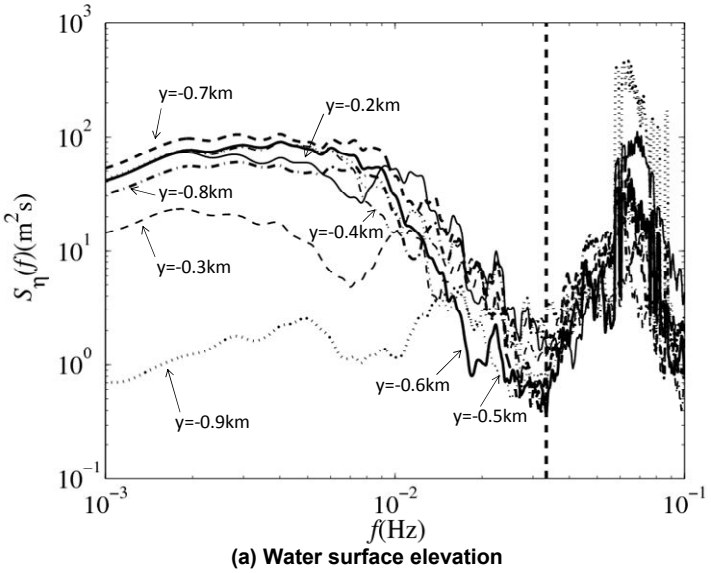

(a) Water surface elevation

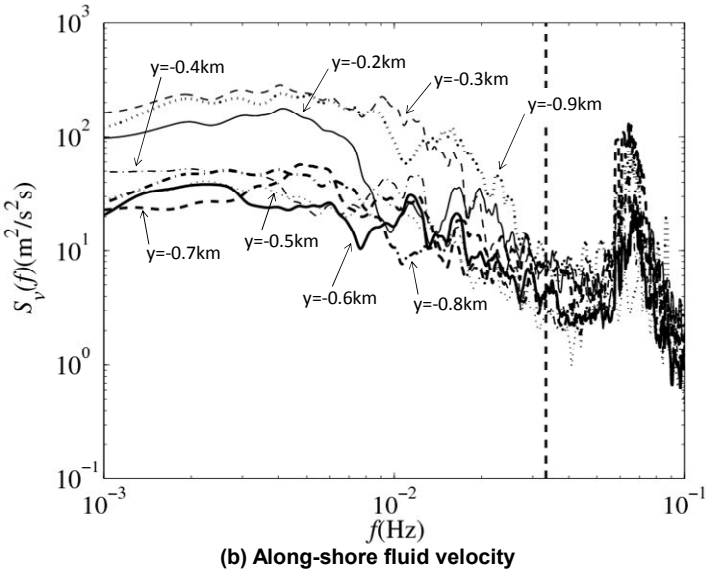

(b) Along-shore fluid velocity

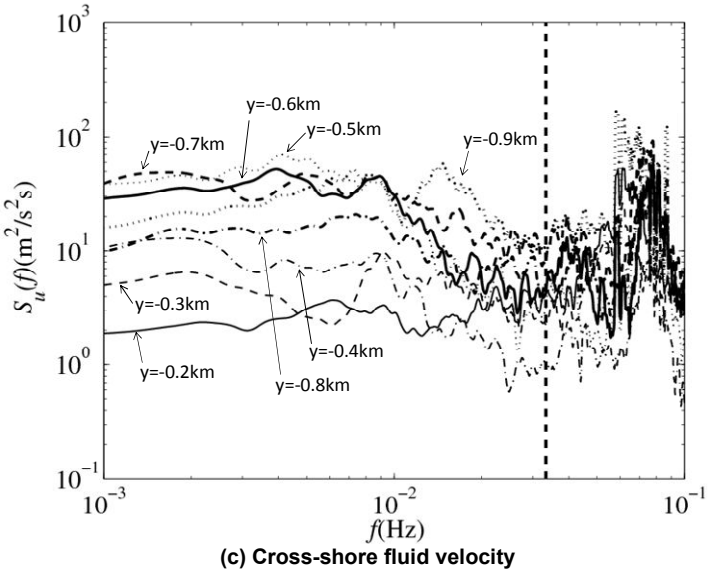

(c) Cross-shore fluid velocity

Figure 8. Spectra of water surface elevation and fluid velocity in front of seawall

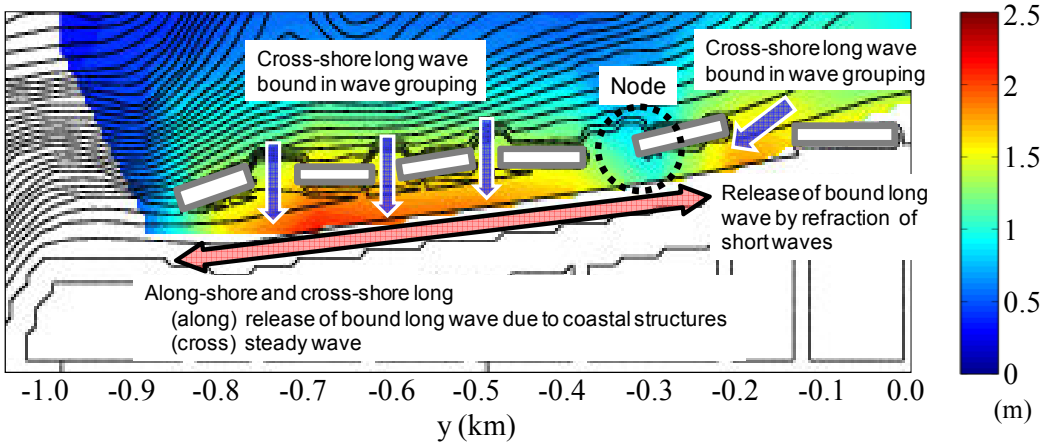

Figure 9. Behavior of long waves in front of seawall (contour: long wave height)

(i.e., $S_v = O(10^2)$) near $y = -0.3$ km. These results indicate the existence of a standing long wave along the shore which has a node at $y = -0.3$ km. However, the energy density of the cross-shore fluid velocity for the long waves is extremely small. The reason for this is thought to be that the waves with wave grouping refract on the sharply changing coastal bathymetry around $y = -0.3$ to -0.2 km and the free long waves released from wave groupings propagate along the shore. These results are supported by the finding that the phase of the long waves is in good agreement with one of the enveloped waves for the short waves as shown in the previous section. Thus, it is estimated that the along-shore long waves are generated on the mild slope side around $y = -0.3$ to -0.2 km. Second, on the steep slope side around $y = -0.8$ to -0.4 km, the energy densities of both two-directional fluid velocities for the long waves are large (i.e., S_u and $S_v = O(10^1)$ to $O(10^2)$). It is estimated that not only the along-shore long waves but also the cross-shore long waves based on the short waves from offshore are generated simultaneously. This result is supported by the finding that even though the phases of the enveloped waves for the short waves from $y = -0.8$ to -0.4 km mutually correspond among each measurement point, there is a significant difference in profile between the long waves and enveloped waves for the short waves. Therefore, the long waves on the steep slope side are generated by the superposition between the along-shore and cross-shore long waves spatially. The behavior of the long waves in front of the seawall is summarized in Fig. 9.

Effective Countermeasures for Wave Overtopping

In the previous section, we investigated the characteristics of wave transformation and wave overtopping around the damaged area. In particular, it was supposed that the generated long waves and wave set-up on the steep slope side and the increase of the short waves due to the local wave concentration on the mild slope side have adverse influences on the increase of wave overtopping. This section examines the effects of countermeasures for wave overtopping based on the above characteristics.

Two types of countermeasure were selected to evaluate their effect on reducing the wave overtopping rate. One was an impermeable jetty installed at the border between the mild and steep slope sides ($y = -0.3$ km), with dimensions of 194 m long, 11.0 m wide and 3.0 m high above the still water level (Fig. 10(a)). The water depth at the head of the jetty is 20.0 m. The jetty is expected to control the long waves which propagate along the shore from the mild to steep slope side. The other countermeasure is two impermeable submerged breakwaters installed at the depth of 20.0 m on the mild and steep slope sides at a little distance from the seawall, with dimensions of 117 m long, 45.0 m wide and 5.0 m deep below the still water level (Fig. 10(b)). These submerged breakwaters are expected to control the wave concentration set-up of the short waves propagating from offshore.

Fig. 11 shows the characteristics of the wave transformation in front of the seawall and the wave overtopping rate for the two types of countermeasure. The open and filled circles indicate the data without and with each countermeasure, respectively. Fig. 11(a) shows that the wave overtopping rate at $y = -0.3$ km decreases with decreasing short and long wave height, and variation of wave set-up by placing the jetty because of the shielding effect of the jetty. On the other hand, the wave overtopping rate at $y = -0.2$ km increases because of the reflected waves at the jetty. Moreover, the long wave

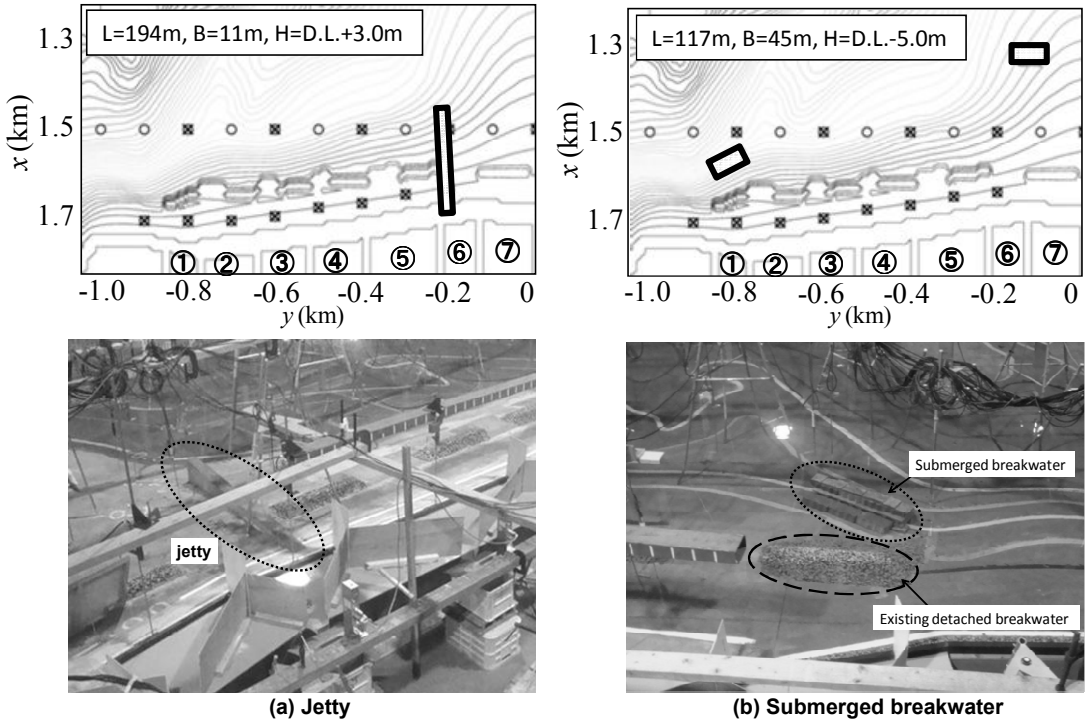

Figure 10. Location of countermeasures for wave overtopping

heights and variations of wave set-up decrease from 0.3 to 1.0 m and from 0.1 to 0.5 m on the steep slope side around $y = -0.7$ to -0.4 km by placing the jetty, respectively. However, as the distance from the jetty increases, its reduction effects gradually decreases and one of the wave overtopping rates is approximately 5 % in the most severely damaged area ($y = -0.8$ km). These results imply that the jetty may control the behavior of long waves along the seawall, but the range of reduction effect is limited to the area surrounding the jetty. On the other hand, the wave overtopping rate decreases substantially in the most severely damaged area due to the decreased wave set-up as shown in Fig. 10(b), although there is little difference between the short and long wave heights with and without the two submerged breakwaters around $y = -0.7$ to -0.5 km. The effect of the submerged breakwaters on reducing wave overtopping rate is approximately 30 % in the most severely damaged area.

CONCLUSIONS

In this study, model experiments were conducted by using a large basin to investigate the mechanism and countermeasures of wave overtopping for long-period swells at the Shimoniikawa Coast. The main conclusions are as follows:

1. Long waves induced by wave groupings and wave set-up affect wave overtopping on the steep slope side and short waves with wave groupings affect wave overtopping on the mild slope side.
2. It is possible to decrease wave overtopping discharges of long-period swells by placing a jetty or some submerged breakwaters to control along-shore long waves in front of a seawall or short waves with wave groupings propagating from offshore.
3. When discussing countermeasures for wave overtopping of long-period swells, it is important to consider the effects on not only short waves but also long waves and wave set-up.

ACKNOWLEDGMENTS

This research was partially supported by the Japan Railway Construction, Transport and Technology Agency.

REFERENCES

Fukase, Y., R. Suminda, Y. Tajima and S. Satoh. 2009. Deformation of long-period giant waves on the Shimoniikawa coast, *Journal of JSCE, Ser. B2 (Coastal Engineering)*, Vol.65, 1411-1415 (in Japanese).

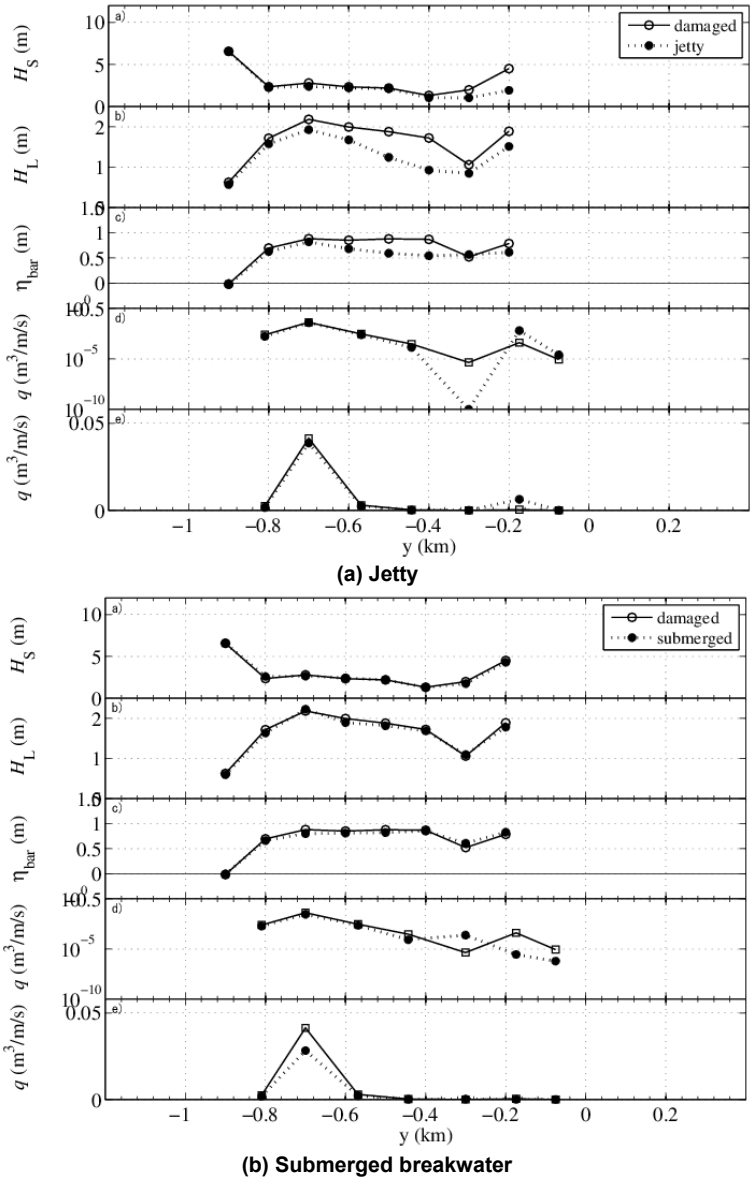

Figure 11. Reduction effects of countermeasures (H_S: short wave height, H_L: long wave height, η_{bar}: mean water surface elevation rising, q: wave overtopping rate (upper: log value, lower: normal value))

Fukase, Y., R. Suminda, Y. Tajima and S. Satoh. 2010. Mechanism and countermeasures for local amplification of long period waves due to alongshore change in nearshore bathymetry, *Journal of JSCE, Ser. B2 (Coastal Engineering)*, Vol.66, 21-25 (in Japanese).

Hirayama, K., H. Kashima and T. Hiraishi. 2008. Examples of unexpected high waves in shallow water in Japan, *Proceedings of Rogue Waves 2008*, 49-58.

Hirayama, K., H. Kashima and K. Nakai. 2009. A study on characteristics of long period swell spectrum and its grouping, *Annual Journal of Civil Engineering in the Ocean*, JSCE, Vol.25, 635-640 (in Japanese).

Janssen, T. T. and J. A. Battjes. 2003. Long waves induced by short-wave groups over a sloping bottom, *Journal of Geophysical Research*, Vol.108, C8, 14 pp.

Kashima, H., K. Hirayama, T. Hiraishi and K. Shimizu. 2009, Estimation of encounter timing of swell by using nationwide wave observation system (NOWPHAS), *Technical Note of The Port and Airport Research Institute*, No.1191, 21 pp. (in Japanese).

Kashima, H. and K. Hirayama. 2009. Effects of bottom topography characteristics on transformations of long period swell, in: *Proceedings of the 4th SCACR - International Short Conference on Applied Coastal Research*, 197-205. ISBN 978-3-00-030141-4. Barcelona, Spain.

Kashima, H. and K. Hirayama. 2010, Experiments on wave overtopping rate and wave pressure on seawalls of long period swell, *Technical Note of The Port and Airport Research Institute*, No.1218, 26 pp. (in Japanese).

Kawasaki, K., N. Mizutani, K. Iwata, T. Kobayashi, M. Yuhi, T. Saitoh, T. Kitano, H. Sumi, H. Mase and T. Yasuda. 2008. Field survey of damage due to February 2008 high wave on east coast of Toyama Prefecture, *Annual Journal of Coastal Engineering,* JSCE, Vol.55, 151-155 (in Japanese).

Tajima, Y., H. Ishizashi and S. Satoh. 2009. Concentration of slowly-varying nearshore waves and currents around the edge of two different bottom slopes, *Journal of JSCE, Ser. B2 (Coastal Engineering)*, Vol.65, 211-215 (in Japanese).

List, J.H. 1992. Wave groupiness variation in the nearshore, *Coastal Engineering*, Vol.15, 475-496.